# *Detection of Zn in water using novel functionalised planar microwave sensors*

Ilaria Frau[a]*, Steve Wylie[a], Patrick Byrne[b], Jeff Cullen[a], Olga Korostynska[c], Alex Mason[a,d,e]

[a]Faculty of Engineering and Technology, Liverpool John Moores University, Liverpool L3 3AF, UK

[b]Faculty of Science, Liverpool John Moores University, Liverpool L3 3AF, UK

[c]Faculty of Technology, Art and Design, Department of Mechanical, Electronic and Chemical Engineering, Oslo Metropolitan University, Oslo, Norway

[d]Animalia AS, Norwegian Meat and Poultry Research Centre, PO Box Økern, 0513 Oslo, Norway

[e]Faculty of Science and Technology, Norwegian University of Life Sciences, 1432 Ås, Norway

[*]i.frau@2016.ljmu.ac.uk, Byrom Street, Liverpool L3 3AF, UK

**Abstract**

Metal pollution in aquatic environments has attracted global attention. Current methods are not able to monitor water quality in-situ at low-cost. This paper reports on a novel approach for detecting changes in the concentration of zinc in water using electrical and a microwave sensor method, adopting two planar sensors: one was functionalised with a screen-printed β-$Bi_2O_3$ based coating, while the other was uncoated. Results show that both electrical and the microwave sensor responses were dependent on the presence and concentration of Zn in water with $R^2$ = 0.93-0.99. The functionalised sensor with a 60 µm thick β-$Bi_2O_3$ based film offers improved performance compared with both uncoated and functionalised sensors with 40 µm thick coating for detecting the changes of Zn concentrations in water for low levels (100 and 500 µg/L). This novel sensing system could be a cost-effective alternative to the current offline methods.

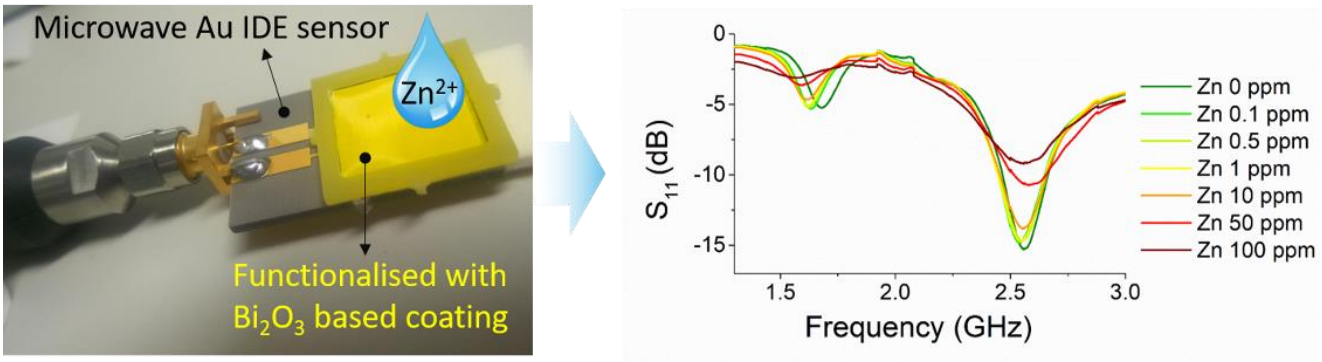


**Keywords**

- Microwave sensing system
- Zinc detection
- Functionalised EM planar sensors
- Water quality monitoring
- Bismuth (III) oxide thick film
- Screen printing

## 1. Introduction

Extraction and processing of metal-bearing minerals has caused global environmental problems, due to the dispersion of toxic metals (zinc, lead, cadmium, copper) which are neither degraded nor destroyed by micro-organisms [1]. Therefore they persist in the environment and can migrate and accumulate in various media under different geochemical and hydrological settings that may directly or indirectly impact plants, animals and humans [2].

In mining regions, zinc (Zn) is one of the most common trace metals found in surface waters and is a worldwide human [3] and environmental health concern [4]. Generally, the ionic form of Zn ($Zn^{2+}$) is considered most toxic. However, other weakly complexed species (oxides, hydroxides and sulphates) and organic colloidal phases are also a cause for concern. Zn will exist primarily in ionic form at pH < 4.5 and will precipitate or sorb to other phases as the pH increases [5]. Globally, Zn concentrations in mine water can be greater than 500 mg/L, with typical concentrations ranging from 0.1 to 10 mg/L [6]. Environmental standards for Zn are derived from the UK Technical Advisory Group on the Water Framework Directive (UKTAG) and the U.S. Environmental Protection

Agency, which established limits of environmental quality standard (EQS) for the Zn in surface water respectively of 8-125 µg/L and 59-210 µg/L [7, 8].

There are numerous examples documenting the environmental impact of mining and metal pollution on water resources and animal and human health [9]. In 2015, a major failure of the Fundão and Santarém mine tailings dams in Minas Gerais, Brazil, caused a release of 62 million $m^3$ of sediment and water into the Rio Dulce and the Atlantic Ocean (approximately 650 km of rivers were impacted). Furthermore, historical mining in the Rio Tinto Mining district, Spain, for more than 5000 years, has polluted more than 90 km of the Rio Tinto with extremely high concentration of metals and low pH (<3): 8.1% of the global dissolved Zn flux in rivers come from the Rio Tinto [1].

It is difficult to characterise water resources accurately in polluted mining areas *in situ* [10]. This is a problem because the current methods available for evaluating the state of Zn-polluted water are laboratory-based spectroscopic techniques that include: atomic absorption spectroscopy (AAS), inductively coupled plasma – optical emission spectrometry (ICP-OES), inductively coupled plasma - mass spectrometry (ICP-MS) and instrument neutron activation analysis (INAA) [11]. Although these techniques have advantages such as the low limit of detection, high sensitivity and the possibility to detect simultaneously a large range of metals simultaneously, they suffer from some drawbacks: they are bulky, require of costly chemicals, and necessitate the use of specialised staff to operate them [12]. The fact that they are offline means they are not able to provide early warning of contamination events or provide the spatial and temporal data resolution necessary to advance our understanding of toxic metal dynamics in river catchments. Therefore, proper impact assessment and an appropriate remediation strategy, based on adequate water properties monitoring using advanced sensor technologies are essential steps for the optimal environmental management and polluted water remediation [4].

The Water Framework Directive (WFD) and the Clean Water Act (CWA) are the major bodies of legislation for the protection and sustainable use of European and United States freshwater resources respectively, which in turn creates the need for low-cost continuous monitoring technologies [13]. Accordingly, research have been carried out to monitor and analyse the impact of Zn ion toxicity in the environment [14]. The dominant areas of development of sensing technologies to measure the concentration of Zn in water include optical fiber sensors [15-17], biosensors [18, 19], and electrochemical sensors [20-22].

No single system available today can fully address the needs of monitoring the concentration of Zn in water resources, continuously and in real time, to the desired sensitivity level, bearing in mind the requirement for system portability and cost-effectiveness. Therefore, novel real-time monitoring techniques are necessary. One technique potentially capable of meeting this current demand is based on microwave sensing [23], as presented in this paper.

## 2. Microwave sensing system

### *2.1. Operation principle of a traditional microwave sensor*

The principle is based on the interaction of propagating or resonating EM (electromagnetic) waves with the material under test. The amplitude and phase of the reflection coefficient ($S_{11}$) (Fig. 1) will vary depending on the properties of the analyte presented to the sensing structure. These properties can be described in terms of electrical parameters such as conductivity, capacitance, resistance, inductance and permittivity. Their combination is strongly related to the material composition at specific frequencies. The novel approach considers how a change in the $S_{11}$ signal can be linked to the type and amount of the pollutant in the water sample being tested. The response of the sensor manifests itself as a resonant frequency change, alteration in the signal amplitude or a resonant peak shift [24].

Microwave planar printed patterns for various sensing applications are increasingly used due to their versatility, flat profile, small size and weight. Their design can be tailored to suit particular applications, coupled with reliability and cost-efficiency. Another distinct advantage of this novel sensor is that typical sample volumes are 400 µL for the test and no additional chemicals are required - a feature not available with comparable methods.

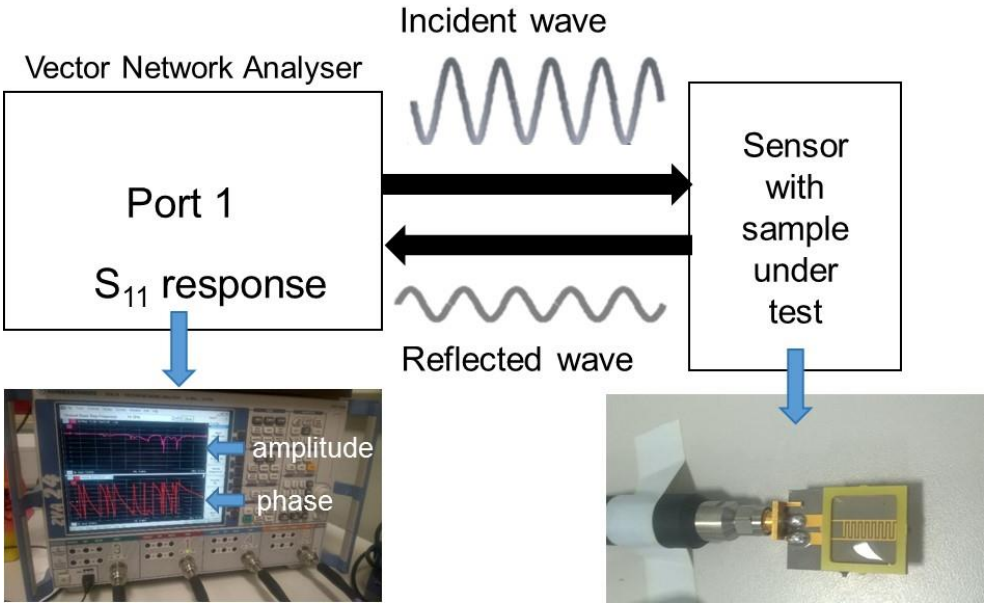


**Fig. 1.** Scheme of the $S_{11}$ responses (amplitude and phase).

The real-time nature of the measurements and potential portability of the sensor makes the suggested approach a valuable alternative to lab-based methods of a wide range of applications including health monitoring [25] and quality control in the food industry [26], and environment [27, 28]. In recent years, the authors have demonstrated a number of possible uses of such devices in water quality analysis, particularly in relation to wastewater [29, 30].

### *2.2. Functionalising EM sensors*

Cheap, sensitive and selective sensor to monitor Zn-impacted water, is achieved by the integration of a chemical coating onto planar interdigitated electrodes (IDE) sensors using screen-printing technology [31], which is known for its flexibility and cost-effective mass production [32]. Thick films are rugged, reproducible, cost-effective and have also been identified as useful for integration into remote monitoring systems [33]. By functionalising planar sensors with certain materials that are specifically sensitive to the pollutant of interest in a water sample, it is possible to obtain the desired sensitivity and/or selectivity of the water quality monitoring system. This can be achieved not only with the adoption of the appropriate mix of materials, but also by choosing the optimal thickness of the film and the sensor geometry [34, 35].

The synergy between microwave sensing technology and chemical material is still at a premature stage with certain advantages deemed to be of interest [36]. Among these, nanomaterials as inorganic oxide compositions are considered to be most advantageous, owing to their strong adsorption and rapid electron transfer kinetic [12, 37].

Recently, a number of approaches make use of Bi based electrodes [38], which has replaced the mercury electrode mostly in electrochemistry for the detection of trace metals due to their low toxicity, excellent resolution of neighbouring peaks, and their low limit of detection toward metals (<0.1 µg/L) [39]. The modification of graphite screen-printed electrodes with a bismuth oxide ($Bi_2O_3$) precursor has been showed in several experiments to have superior sensing characteristics toward metals compared to Bi bulk electrodes [40, 41].

In an effort to combine the benefits of both approaches, in this work, gold IDE sensors were functionalised with β-$Bi_2O_3$ based thick-film with the purpose of increasing the reaction and consequently the sensitivity and selectivity between Zn water solutions and the sensing material.

The objectives of this work are 1) to measure changes in electrical parameters (capacitance and resistance) for Zn concentrations in water; 2) to evaluate the feasibility of using microwave techniques for detecting Zn in water solutions, especially in the critical concentration range 0-1 mg/L; 3) to compare responses obtained with uncoated and functionalised EM sensors with $Bi_2O_3$ based film at different thicknesses.

## 3. Materials and Methods

### *3.1. Paste mixture preparation and thick film properties*

The functionalised EM (f-EM) sensors were prepared by screen-printing using a semi-automatic screen-printer (Super Primex) to coat a paste mixture based on $Bi_2O_3$ onto gold eight-pair IDE sensors (Fig. 2 a, b, c). The paste mixture was prepared by mixing three materials: 1) a functional material (powder form, 92.5wt.%): bismuth (III) oxide nanopowder 90<Φ<210 nm particle size, tetragonal phase (β-$Bi_2O_3$) and a space group P $\bar{4}2_1c$ (114), (Sigma-Aldrich 637017); 2) an organic binder (solid form, 7.5wt.%): PVB, butvar B98 (Sigma-Aldrich B0154); 3) an organic volatile solvent (liquid form, few drops): ethylene glycol butyl ether (Sigma-Aldrich 579556) [42]. These last two materials operate as a matrix for designing the appropriate consistency to be screen-printed (0.1 to 10 Pa s). The coatings were built by successive printing, with two f-EM sensors having 4 and 6 layers, which correspond respectively on average to 40 and 60 µm, and a set of sensors was left uncoated (Fig. 2 c). The exact thickness was evaluated with an electronic micrometer (TESA Micromaster), a digital vernier caliper (AOS Absolute Digimatic) and a surface profiler (Teylor Hobson - Form Talysurf 120). Each layer was cured in an oven at 170°C for 1 hour between each printed layer.

The repeatability, reproducibility and stability of the coatings screen-printed onto microscope slides, were evaluated by analysing the properties before and after contact with Zn polluted water samples. Optical absorbance, was measured using a UV-Vis Spectrophotometer, Jenway 7315. Structural properties were analysed with a scanning electron microscope, SEM, model FEI - Quanta 200 (Fig. 2 d) and an optical microscope, ZEISS AX10 (Fig. 2 e). Likewise, elemental properties were determined with an X-Ray Fluorescence Analyser, (XRF, model INCA-X-act).

### *3.2. Sample preparation*

Seven samples of Zn in water at different concentrations (0, 0.1, 0.5, 1, 10, 50, 100 mg/L) were prepared by dissolving a defined volume of Zn 1000 ppm ICP standard solution certified (Sigma-Aldrich 18562, 1000 mg/L Zn in 2% nitric acid, prepared with high purity Zn metal, $HNO_3$ and water) in deionised water. The specific conductivity of the Zn solutions was measured using a conductivity meter (PCE-PHD 1, PCE Instruments) and described in Table S1. All measurements were performed in an air-conditioned environment at a constant temperature of 20°C.

### *3.3. Electrical and electromagnetic measurements*

Zinc solutions were analysed with a programmable LCR meter and microwave spectroscopy. Capacitance ($C_p$) and resistance ($R_p$) were measured using a HAMEG 8118 LCR (L = inductance; C = capacitance; R = resistance) bridge configured with a bespoke coaxial probe at a frequency range between 20 Hz and 20 kHz, with constant 1.00 V open circuit voltage and using a LabVIEW software interface (Fig. 3 a, b, c). A gold-plated sensing structure with two electrodes was used for measuring 400 µL of sample volume, held in place by a designed holder integrated onto a microscope slide (Fig. 3 d). Five repetitions were performed for each Zn concentration.

In this work, three sets of gold eight-pair IDE pattern printed on planar PTFE substrates were used: one sensor was uncoated and the other two were functionalized (as described in the section *3.1.*). The microwave IDE sensors were connected to a Rohde and Schwarz ZVA 2.4 VNA (Vector Network Analyser) via a coaxial cable (Fig. 3 e). Molex edge mount connectors were used in this work as SMA type connectors. All the equipment was specified for 50 Ω impedance. The VNA used a one-port configuration to enable $S_{11}$ measurements, in the 10 MHz – 15 GHz frequency range (60,000 discrete points). For each measurement (n=5 for each concentration), 400 µL of Zn

solution was dispensed onto the sensor using a pipette, with the solution held in place by a well – a holder manufactured specifically for these sensors.

For each technique and Zn solutions (0-100 mg/L) the coefficient of determination ($R^2$), the sensitivity for each 100 mg/L changes of Zn (as the slope of the calibration curve), and the precision, as the relative standard deviation (RSD, %) were measured. The RSD is the ratio of the standard deviation to the mean.

*3.4 Adsorption experimentation*

The absorption of the Zn ions on the coating was estimated by performing a sorption experiment as described by Dada, Olalekan [43] and modified as Frau, Wylie [44]. Part of thick-films screen printed on microscope slides was immersed on each Zn solution (0.02 g, 2x2 $cm^2$, as the coatings, Fig. S3). The concentration change was estimated by measuring the difference in conductivity ($R^2$=1 for conductivity and Zn concentration, Table S1) before and after 5 and 10 minutes. From this difference, it is possible to estimate the percentage of adsorption of Zn ions on the f-EM sensor substrate.

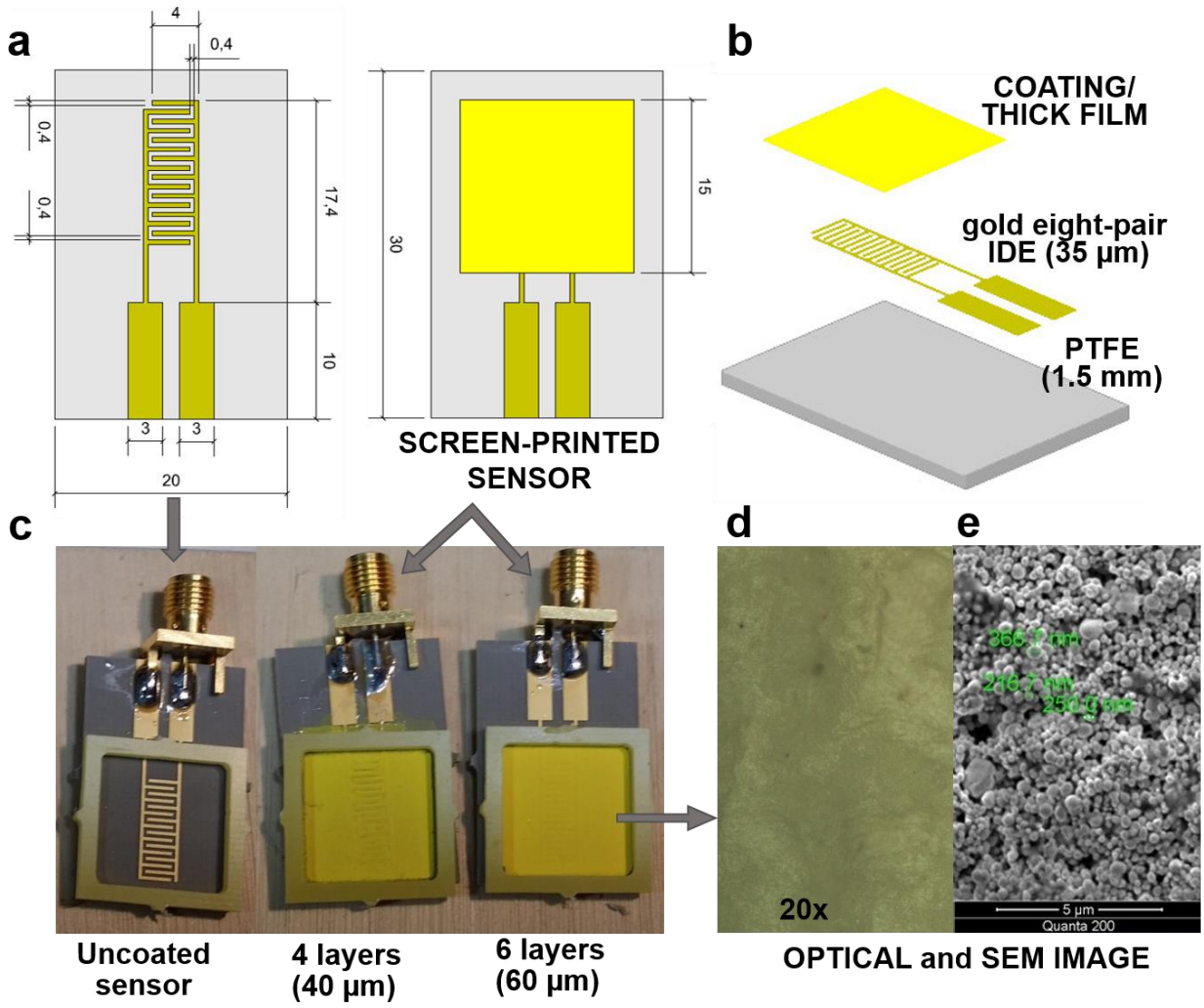


**Fig. 2. (a)** Sizes of the gold pattern and the aspect of the coated sensors (all dimensions are expressed in mm); **(b)** 3D schematic drawing of a functionalised planar gold eight-pair IDE sensor on PTFE substrate with displayed thicknesses; (**c)** the three sensors used in this experiment (from left: uncoated sensor and with 40 and 60 µm of $Bi_2O_3$ based coating; (**d)** an optical (x20) and (**e)** a SEM image of the morphological substrate of the coating where are highlight the particle sizes, resulting between 90 and 400 nm.

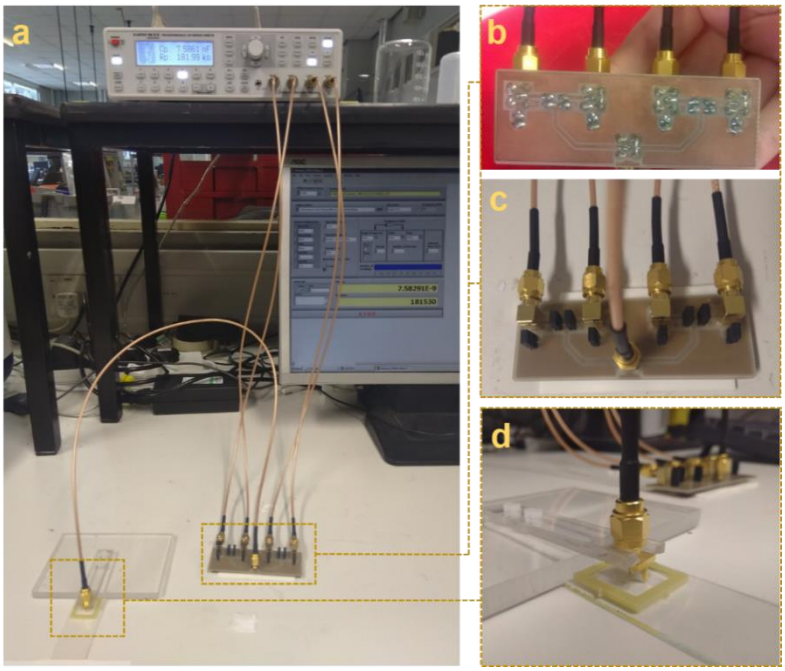


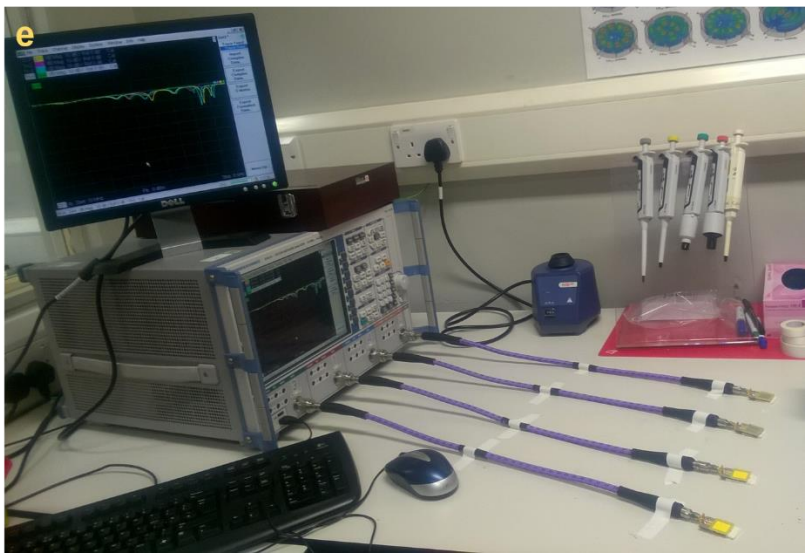


**Fig. 3.** Experimental setup: **(a)** LCR bridge and LabVIEW software interface with a bespoke coaxial probe (assembled with a FR4 circuit board as shown in (**b**), back view, and (**c**), front view) measuring a water sample (400 µL) held in place by a specific holder (as magnified in (**d**). (**e**) Vector Network Analyser (VNA) with coaxial cables to uncoated and functionalised planar sensors with 60 µm $Bi_2O_3$ based coating.

## 4. Results and discussion

### *4.1. Results*

Results obtained measuring the Zn solutions at different concentration with the techniques previously described are summarised in Table 1, which shows $R^2$, sensitivity (for each 100 µg/L of Zn concentration) and

relative standard deviation (RSD) in order to demonstrate the repeatability and reproducibility of the measurements. Spectral responses for capacitance and resistance at the investigated frequencies (20 Hz – 20 kHz) for Zn concentrations 0-100 mg/L are illustrated in Fig. S1 a and S2 a: it is notable how the capacitance and resistance reflect an inverted behaviour. The capacitance increases how the Zn concentration and the specific conductivity increase (Table S1), conversely the resistance decreases. Moreover, the $C_p$ decreases moving towards higher frequencies, contrariwise the $R_p$ remains stable. The part of the spectrum that shows a higher relation between these two parameters and Zn concentration was identified between 200 and 600 Hz (magnified in Fig. S1 b and S2 b). Two frequency were selected as representative of this this frequency range for assessing the correlation between $C_p$ and $R_p$ and Zn ion concentration (250 Hz and 500 Hz, respectively).

Low-frequency electrical measurements were able to detect changes in Zn concentration. The capacitance measurements show a good linear correlation with Zn concentration at 250 Hz, with $R^2 = 0.9991$. Otherwise, the resistance and Zn concentration are correlated with a power trend with $R^2 = 0.9468$ at 500 Hz. Fig. 4 shows these two electrical parameters where Zn concentration is expressed with a logarithmic scale to permit to distinguish also a calibration curve under 1 mg/L (0.1 and 0.5 mg/L).

**Table 1** Summary of statistical features obtained for optical, electrical and microwave measurements of Zn water sample

| Properties | | $R^2$ | Sensitivity[a] | RSD (%) |
|---|---|---|---|---|
| Capacitance (at 250 Hz) | | 0.9991 | 0.5 nF | 2.5 % |
| Resistance (at 500 Hz) | | 0.9468 [b] | 119.9 Ω | 2.5 % |
| Reflection coefficient ($S_{11}$) - uncoated IDE sensor | at 502 MHz | 0.9914 | 0.0035 dB | 0.6 % |
| | at 1.26 GHz | 0.8377 | 0.0014 dB | 0.6 % |
| | at 2.46 GHz (peak) | 0.9563 | 0.0065 dB | 1.1 % |
| Reflection coefficient ($S_{11}$) – functionalised IDE sensor (4 layers, 40 µm) | at 511 MHz | 0.9915 | 0.0032 dB | 1.3 % |
| | 1.26-1.35 GHz | 0.8301 | 0.0018 dB | 1.1 % |
| | at 2.51 GHz (peak) | 0.9682 | 0.0054 dB | 2.1 % |
| Reflection coefficient ($S_{11}$) – functionalised IDE sensor (6 layers, 60 µm) | at 599 MHz | 0.9993 | 0.0028 dB | 1.8 % |
| | 1.57-1.68 GHz | 0.9318 | 0.0022 dB | 2.0 % |
| | at 2.56 GHz (peak) | 0.9466 | 0.0069 dB | 2.8 % |

[a] for every 100 µg/L change of Zn concentration; [b] power correlation;

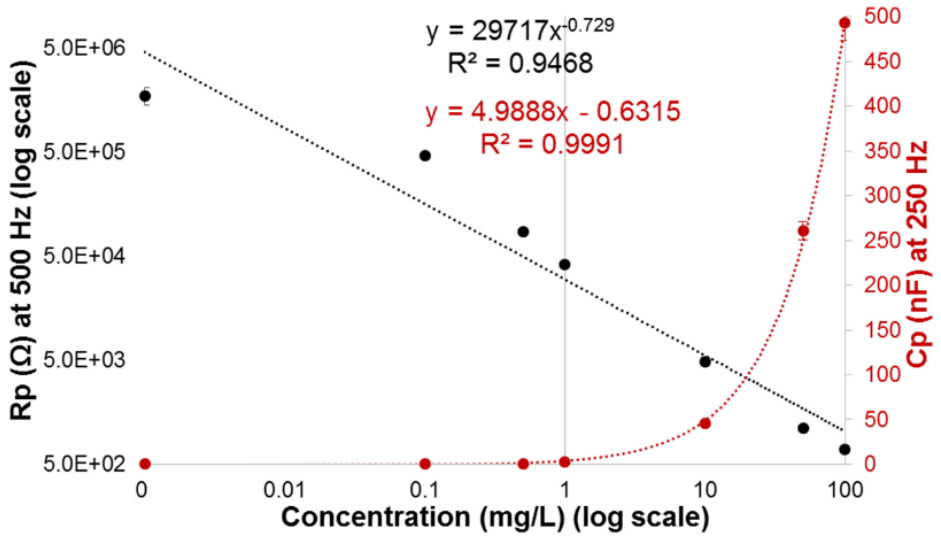


**Fig. 4.** Power correlation between resistance ($R_p$) (expressed in logarithmic scale) and Zn concentration (log scale) (in black) at 500 Hz; and linear correlation between capacitance ($C_p$) and Zn concentration (log scale) (in red) at 250 Hz. Both parameters are measured with an LCR meter.

The adsorption reaction principle and microwave propagation in the whole sensing structure are illustrated in Fig. 5, which shows a cross session of the f-EM sensor with a Zn sample and the propagation of the EM field with electric and magnetic field lines. Zn ions are adsorbed onto the $Bi_2O_3$ based thick-film. The EM field interacts with each component of the f-EM sensor and the change in spectral response will depend on the changes in permittivity that is related with the Zn adsorption onto the coating. The permittivity of the coating material after the adsorption of the Zn will determine a change in permittivity that determines a variation in the spectral response equally to a shift in frequency and/or amplitude.

The absorption experiment estimates that about 4% of Zn is adsorbed on the coating after 5 minutes and 6 % after 10 min (Table S2). This was the time estimated of the interaction between the $Bi_2O_3$ film and the Zn solutions to reach adsorption equilibrium [44]. However, it is probable that the EM wave promotes the adsorption of Zn ions onto the sensing surface.

The elemental pattern (Fig. 6 a) and its percentage composition (Fig 6 b), were determined with the XRF after its use, to confirm the presence of Zn ion in the sensitive layer adsorbed by the coating. This was determined after 2h of continuous measurements and 10 mg/L of Zn concentration sample, considering that the used XRF was not able to determine the presence of Zn ions after short usage and using samples with low Zn concentration,

due to instrumental sensitivity limitation. More experimental work will be performed for a more accurate understanding of the Zn adsorption at low concentration (e.g. performing X-ray photoelectron spectroscopy (XPS) analysis) and the maximum capacity that the f-EM sensor can adsorb before reaching a saturation level.

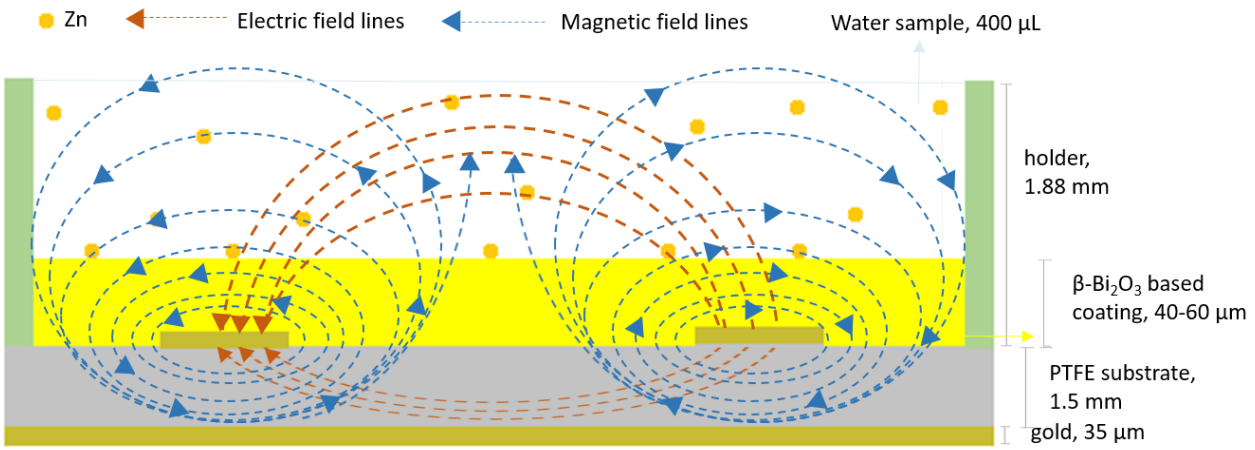


**Fig. 5.** Partial cross-section of the functionalized sensor illustrating schematically the sorption sensing principle and the propagation of the EM field, showing the two components: electric and magnetic fields.

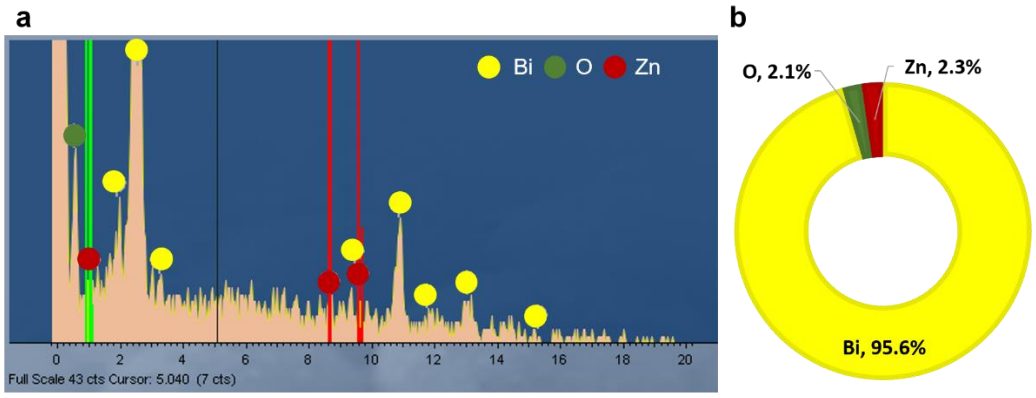


**Fig. 6. (a)** Elemental spectra of the film after the adsorption and **(b)** the relative elemental weight % of sensing layer surface using 10 ppm Zn solution.

The response for the microwave technique with uncoated and coated sensors demonstrates a shift in signal amplitude, which corresponds to the different concentrations of Zn tested. During the measurements, significant resonant peak shifts were noticed for the different concentrations of Zn ions in water as soon as they were in contact with the EM field through the sensing structure. The distinct feature is the change in the resonant peak amplitude, clearly visible in several parts of the spectrum, especially between 100 MHz and 3 GHz, with the

amplitude decreasing with increasing Zn concentration, for peaks at frequency < 1 GHz, and increasing for peaks identified > 1 GHz. Fig. 7 and 8 illustrate the $S_{11}$ magnitude respectively of the uncoated microwave sensor and one coated with 60 µm $Bi_2O_3$ based thick film in contact with various Zn concentration solutions. A number of resonant peaks can be identified to serve as an indicator of the Zn content in a solution. The microwave spectra are different for each Zn solution at various concentrations with the most pronounced resonant peaks, indicating sensitivity, at around 2.5 GHz for all the sensors used. Fig. 9 shows two frequencies and a frequency range (599 MHz, 2.56 and 1.57-1.68 GHz) at which good correlations (respectively $R^2 = 0.9993$, $R^2 = 0.9318$ and $R^2 = 0.9466$) with Zn concentration (expressed with a logarithmic scale to permit to distinguish also 0.1 and 0.5 mg/L of Zn) and $S_{11}$ occur, using the 60 µm $Bi_2O_3$ based sensor. Generally, at the most pronounced peak, the sensitivity is higher, but RSD is higher and $R^2$ is lower than the other points. Consequently, it is advantageous to find an appropriate compromise depending on the particular analysed condition. However, the measurements are precise and repeatable, considering the RSD < to 2.8 % for all performed measurements, lower than the variation for each parameter (ΔnF, ΔΩ, ΔdB) to determine significant changes in Zn concentration. Also, the sensors are reusable, considering that the sensor output returned to its baseline level (air spectra) when Zn polluted water samples were removed and the sensor was rinsed and allowed to dry (Fig. S4). This indicates that planar EM sensors are reliable and reusable, probably due to the weak solubility of metal oxides [45].

By comparing the spectral response between electrical and EM measurements at microwave frequencies, it is notable that microwave multi-peak spectra offer a more specific characterisation of the water samples under test with its high spectral resolution using 60,000 distinct points. Contrariwise, low-frequency capacitance and resistance responses gave a less specific signature, considering their “flat” profile.

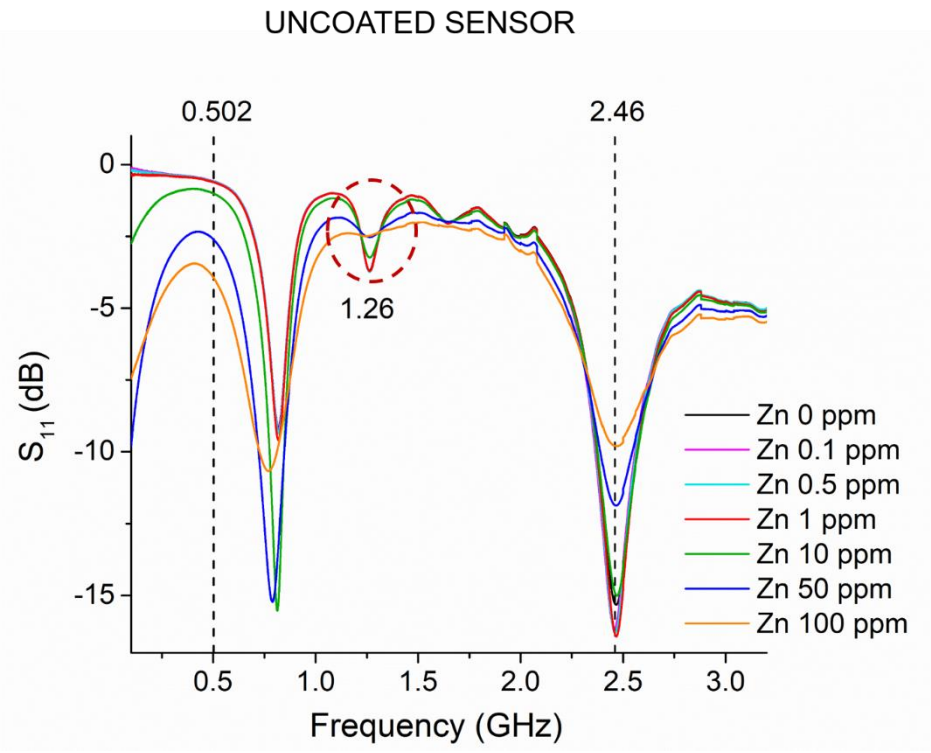


**Fig. 7.** Average microwave spectra data captured with an uncoated gold eight-pair IDE sensor at 0.1 – 3.25 GHz frequency range for each sample concentration of Zn. Three amplitude shift are marked, namely at 0.502, 1.26 and 2.46 GHz (peak).

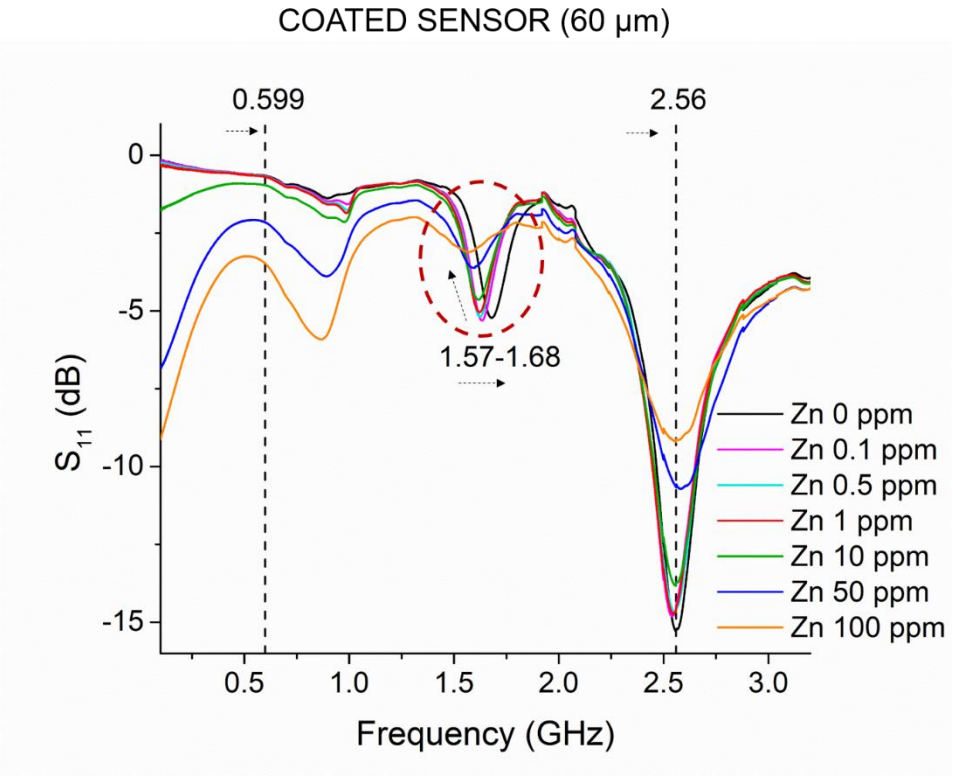


**Fig. 8.** Average microwave spectra data captured with a coated gold eight-pair IDE sensor with 60 µm thickness of $Bi_2O_3$ based film at 0.1 – 3.25 GHz frequency range for each sample concentration of Zn. Two amplitude shift are marked, namely at 0.599 and 2.56 GHz (peak). Between 1.57 and 1.68 GHz is been identified a shift in both, amplitude and frequency.

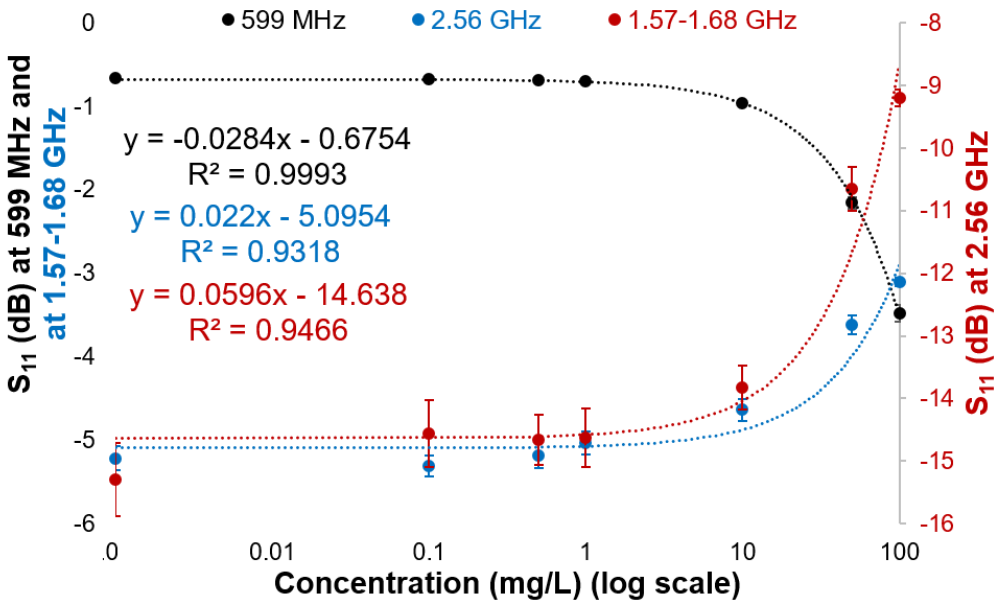


**Fig. 9.** Change in $S_{11}$ of microwave spectra measured with a functionalised sensors with 60 µm $Bi_2O_3$ based coating showing the correlation with metal concentration (in logarithmic scale for showing 0.1 and 0.5 mg/L) at two discrete frequencies and a frequency range, namely 599 MHz, 2.56 GHz (peak) and 1.57-1.68GHz.

*4.2. Effect of the thick-film*

The response changes due to the effect of the $Bi_2O_3$ based thick film has been compared with the uncoated sensors noting significant differences. This functionalisation enhances the sensor performance significantly leading to a higher sensitivity compared to the bare IDE electrode, particularly around 1.5 GHz for Zn detection.

The effect of the $Bi_2O_3$ based thick film produced an overall shift toward higher frequencies (dot-black arrows in Fig. 8), probably due to the decreasing of the dielectric constant [46]. Notably, with the uncoated sensor, the peak was at 2.46 GHz (Fig. 7); with the functionalised sensor (40 µm) at 2.51 GHz; and with the functionalised sensor (60 µm) at 2.56 GHz (Fig. 8). An interpretation of the obtained results suggests a change in dielectric proprieties due to the thickness of the coating [46, 47].

A higher $R^2$ (=0.9993) is identified at 599 MHz and measured with the 60 µm $Bi_2O_3$ based film. Nevertheless, the linear correlation is higher, the sensitivity is slightly smaller than that measured at 502 MHz with the uncoated sensor (respectively 0.0028 and 0.0035 change in $S_{11}$ for every 100 µg/L change of Zn concentration). Possibly, this is due to a permittivity change of the sensitive coating that induces a decrease of the resonant response at the peak, causing a reduction of the amplitude to the signal [48].

Additionally, with the coated sensors, the change in the resonant peak amplitude was accompanied by a gradual shift in the frequency between distinct Zn concentrations, which increases with thickness. Specifically, the uncoated sensor had a resonant peak at 1.26 GHz (Fig. 10 a); the sensor with 40 µm thickness of $Bi_2O_3$ based film manifests a frequency shift for 0-100 mg/L Zn concentrations between 1.26 to 1.35 GHz (Fig. 10 b); with 60 µm, the shift is more pronounced, recognised at 1.57-1.68 GHz (Fig. 10 c). Notably, for higher Zn concentration solutions, the peak is set at lower frequencies, at 1.57 GHz for 100 mg/L and at 1.63 GHz for 0.1 mg/L. Table 1 describes and compares some statistical parameters, for this less pronounced peak: nevertheless the RSD is slightly higher, the $R^2$ and sensitivity are improved due to the adsorption between the Zn ions on the $Bi_2O_3$ based coating (Table S2) and the consequent permittivity change.

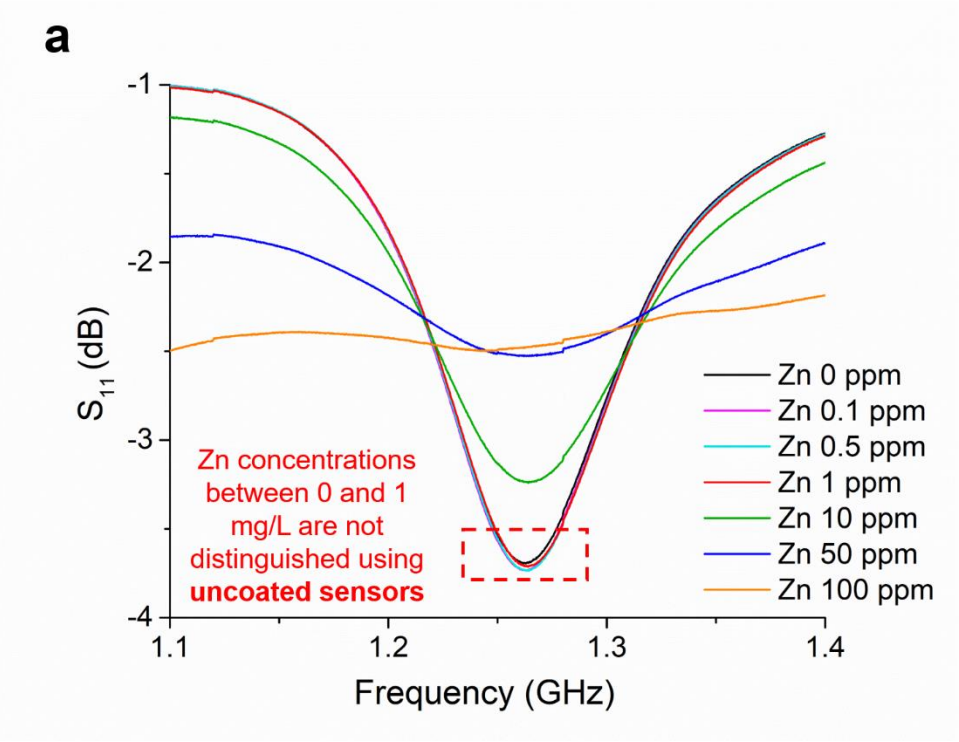

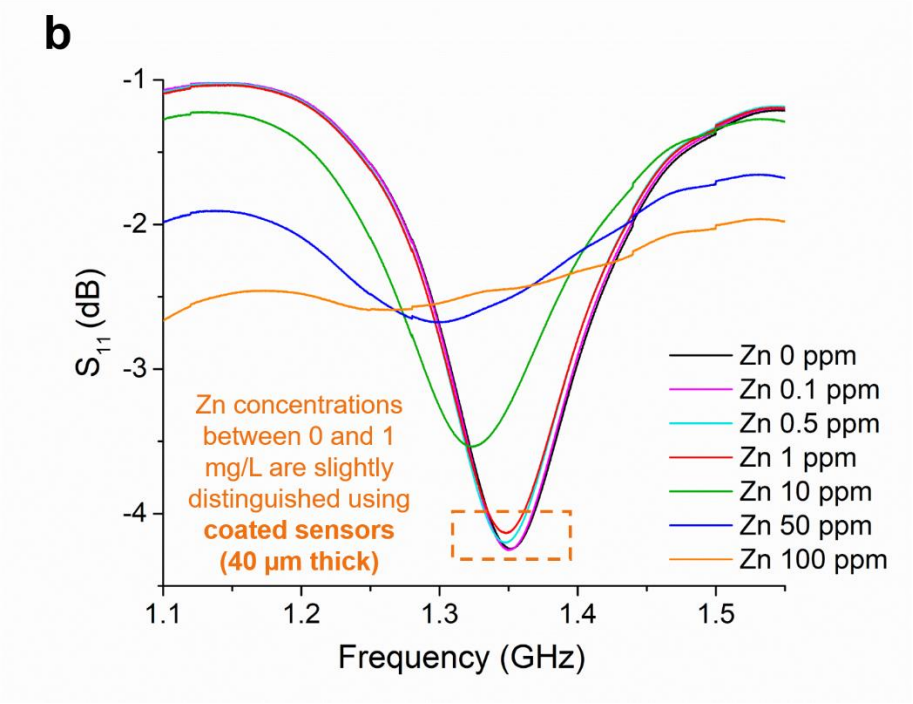


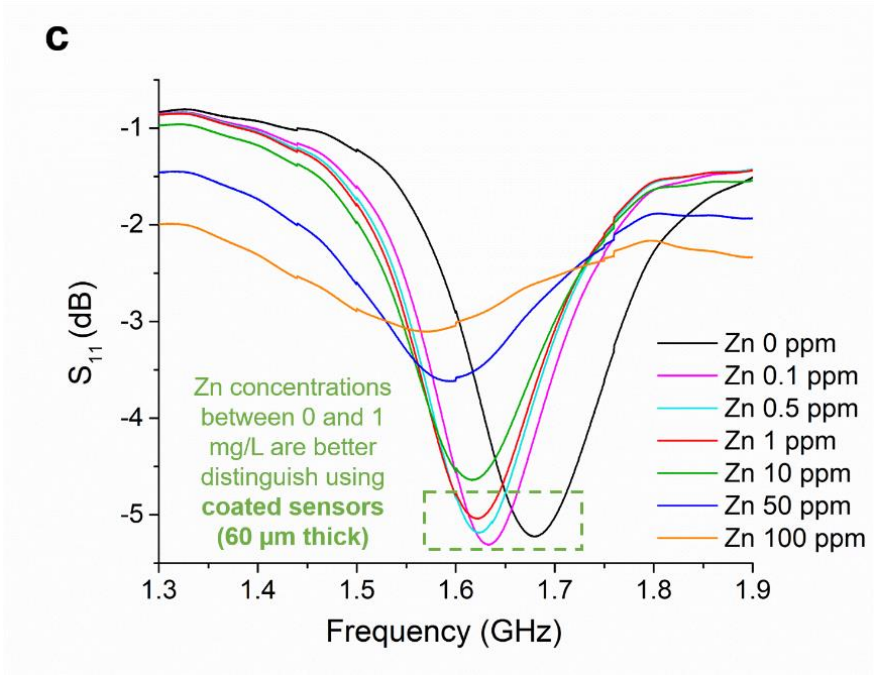


**Fig. 10.** Electromagnetic spectra part focus on the frequencies ranges where it is identified the most pronounced effect of the coating and the increasing in sensitivity measurements for low Zn concentrations (0-1) mg/L: (**a)** spectra from the uncoated sensor, **(b)** 40 µm thickness and (c) 60 µm thickness of $Bi_2O_3$ based coating.

Notably, the sensor response to low-concentration of Zn depends on the thickness of coatings. Due to the shift in both amplitude and frequency, the sensor performance is improved with the 60 µm thick $Bi_2O_3$ based film for all Zn concentrations. Of particular importance is the different response for low concentrations (100 and

500 µg/L) important for detecting Zn level in freshwater superior to the EQSs (> 125-210 µg/L), as highlighted with a red (uncoated sensor), orange (40 µm thick f-EM sensor) and green (60 µm thick f-EM sensor) dash-square respectively in Fig. 10 a, b and c. The f-EM sensor based on 60 µm thick $Bi_2O_3$ film was able to distinguish better 0.1 and 0.5 mg/L of Zn ion concentration in water. Consequently, there is an increase of sensitivity due to this shift in both amplitude and frequency, passing from $1.4x10^{-3}$ dB (uncoated sensor), $1.8x10^{-3}$ dB (40 µm coating) to $2.2x10^{-3}$ dB (60 µm coating) change in $S_{11}$ for every 100 µg/L change of Zn concentration (Fig. 11).

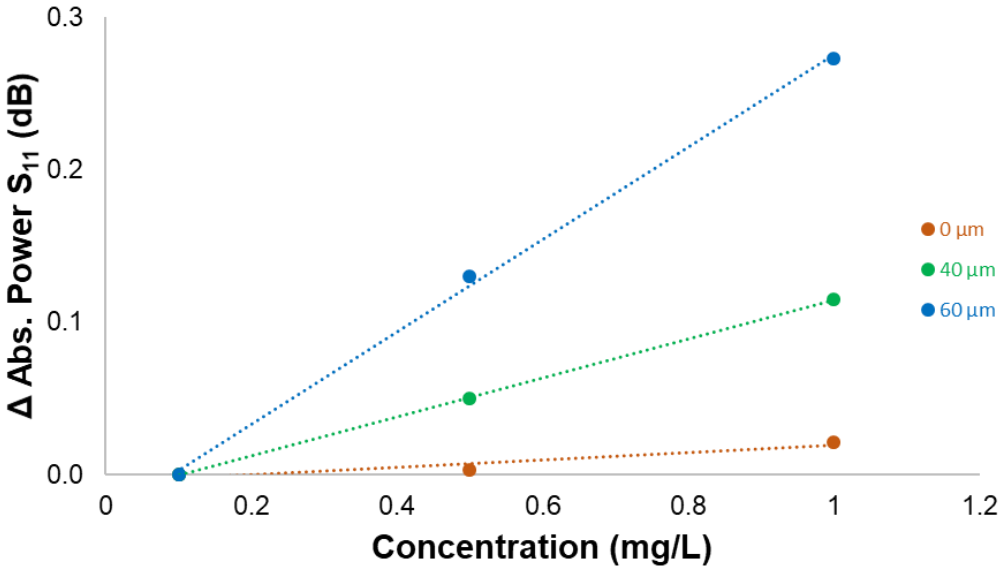


**Fig. 11.** Change in sensitivity with the thickness of the β-$Bi_2O_3$ based coating for Zn concentrations 0-1 mg/L.

These responses are probably due to the effect of a permittivity variation of the sensitive chemical layer [31]. In fact, as described by Bernou, Rebière [48], the electromagnetic wave propagates in each component in the system. Furthermore, the β-$Bi_2O_3$ based film is stable, repeatable and reproducible, as confirmed by absorbance spectra measured of the screen-printed coating on microscope slides.

*4.3. Feasibility of microwave spectroscopy for mine water monitoring and future work*

The experiments presented above confirm that microwave spectroscopy and f-EM sensors could offer a good alternative to the off-line and laboratory-based monitoring technique, which cannot provide a continuous monitoring of Zn and other metal ions in waste water. Microwave spectroscopy using f-EM sensors, which gives an immediate response, could guarantee a continuous monitoring in polluted mining areas and could be employed as an early warning device for contamination events. Moreover, this sensing system could offer a support for

applying a suitable strategy of remediation, considering changes in metal concentration due to alternate rainfall and aridity that influence river stage alternately exposure contaminated river [49, 50].

More work needs to be done to clarify the peculiarities in the chemical and electrical properties of Zn adsorption on the $Bi_2O_3$ based film. An improvement of the synthesis method is also needed to enhance sensitivity and selectivity to different metals, especially in presence of other pollutants and/or different composition of water samples.

Advantages of the use of screen-printing as an application method of functional material are the high diversity of materials that can be processed cost effectively. Another aspect is the possibility of printing a combination of different materials onto the same substrate or part [51]. The designing of the f-EM sensors with best suited architecture will help in increasing selective identification of multi metal ions in water.

There is still considerable work to be conducted in this area, particularly to prove the technology in a real-world scenario. The prototype system will be tested in surface waters and the challenge of differentiating and quantify between unknown multiple water pollutants, namely various toxic metals, will be achieved using cheap portable VNAs connected with f-EM sensors for continuous monitoring polluted mine water on site.

## 5. Conclusion

This research was driven by the global need for developing a novel real-time sensing platform for monitoring Zn in water in abandoned mining areas that would be able to detect unexpected events of pollution and to clarify metal dynamics. The results described in this paper using microwave spectroscopy and f-EM sensors based on $Bi_2O_3$ confirm the potential of this novel combined sensing approach for measuring continuous changes in Zn concentrations in water. Gold eight-pair IDE were functionalised with 40 and 60 μm of β-$Bi_2O_3$ based thick films. Good linear correlations were obtained with electrical and EM measurements and Zn concentration in water (0-100 mg/L). Specifically, the f-EM sensors with 60 μm of $Bi_2O_3$ based thick film, although with a slightly higher RSD (2.0% compared with 1.1% and 0.6% respectively for 40 μm of $Bi_2O_3$ based film and uncoated sensor), provided an improved performance when detecting lower Zn concentrations (0.1 and 0.5 mg/L). This is essential for distinguishing Zn concentrations at the EQS established by global legislation (0-0.2 mg/L).

Further work and field trials are in progress to expand and progress toward the realisation of a sensitive and selective sensor which can offer the ability to monitor continuously various metals simultaneously in water, in-situ and in real-time.

**Acknowledgement**

The authors gratefully acknowledge the support of Liverpool John Moores University, the Faculty of Engineering and Technology in conjunction with the Faculty of Science PhD Scholarship Programme which allowed this research to be undertaken.

**Declaration of interest:** The authors have no conflict of interest.

**Data availability**

The raw data required to reproduce these findings are available on request. The processed data required to reproduce these findings are available on request.

**References**

[1] K. Hudson-Edwards, Tackling mine wastes, Science, 352(2016) 288-90.

[2] X. Zhang, L. Yang, Y. Li, H. Li, W. Wang, B. Ye, Impacts of lead/zinc mining and smelting on the environment and human health in China, Environmental Monitoring and Assessment, 184(2012) 2261-73.

[3] L.M. Plum, L. Rink, H. Haase, The Essential Toxin: Impact of Zinc on Human Health, International Journal of Environmental Research and Public Health, 7(2010) 1342-65.

[4] W.M. Mayes, D. Johnston, H.A.B. Potter, A.P. Jarvis, A national strategy for identification, prioritisation and management of pollution from abandoned non-coal mine sites in England and Wales. I, Science of The Total Environment, 407(2009) 5435-47.

[5] K.S. Smith, Metal sorption on mineral surfaces: an overview with examples relating to mineral deposits1999.

[6] P. Byrne, P.J. Wood, I. Reid, The Impairment of River Systems by Metal Mine Contamination: A Review Including Remediation Options, Critical Reviews in Environmental Science and Technology, 42(2012) 2017-77.

[7] UK Technical Adivisory Group on the Water Framework Directive, UK environmental standards and conditions, https://www.wfduk.org/resources%20/uk-environmental-standards-and-conditions-report-phase-1, 2008.

[8] United States Environmental Protection Agency, Quality criteria for water, Washington, DC 20460: EPA; 1986.

[9] C. Wolkersdorfer, Water Management at Abandoned Flooded Underground Mines — Fundamentals, Tracer Tests, Modelling, Water Treatment, Heidelberg: Springer; 2008.

[10] A. Jones, M. Rogerson, G. Greenway, H.A.B. Potter, W.M. Mayes, Mine water geochemistry and metal flux in a major historic Pb-Zn-F orefield, the Yorkshire Pennines, UK, Environmental Science and Pollution Research, 20(2013) 7570-81.

[11] K.X. Yang, M.E. Kitto, J.P. Orsini, K. Swami, S.E. Beach, Evaluation of sample pretreatment methods for multiwalled and single-walled carbon nanotubes for the determination of metal impurities by ICPMS, ICPOES, and instrument neutron activation analysis, 8 ed., Royal Society of Chemistry2010, pp. 1290-7.

[12] M.B. Gumpu, S. Sethuraman, U.M. Krishnan, J.B.B. Rayappan, A review on detection of heavy metal ions in water – An electrochemical approach, Sensors and Actuators B: Chemical, 213(2015) 515-33.

[13] W. Brack, V. Dulio, M. Ågerstrand, I. Allan, R. Altenburger, M. Brinkmann, et al., Towards the review of the European Union Water Framework management of chemical contamination in European surface water resources, Science of The Total Environment, 576(2017) 720-37.

[14] A. Elzwayie, H.A. Afan, M.F. Allawi, A. El-Shafie, Heavy metal monitoring, analysis and prediction in lakes and rivers: state of the art, Environmental Science and Pollution Research, 24(2017) 12104-17.

[15] W.B. Ji, S.H.K. Yap, N. Panwar, L.L. Zhang, B. Lin, K.T. Yong, et al., Detection of low-concentration heavy metal ions using optical microfiber sensor, Sensors and Actuators B: Chemical, 237(2016) 142-9.

[16] R. Verma, B.D. Gupta, Detection of heavy metal ions in contaminated water by surface plasmon resonance based optical fibre sensor using conducting polymer and chitosan, Food Chemistry, 166(2015) 568-75.

[17] J. Vukovic, M.A. Avidad, L.F. Capitan-Vallvey, Characterization of disposable optical sensors for heavy metal determination, Talanta, 94(2012) 123-32.

[18] I. Gammoudi, V. Raimbault, H. Tarbague, F. Morote, C. Grauby-Heywang, A. Othmane, et al., Enhanced bio-inspired microsensor based on microfluidic/bacteria/love wave hybrid structure for continuous control of heavy metals toxicity in liquid medium, Sensors and Actuators B: Chemical, 198(2014) 278-84.

[19] C. Chouteau, S. Dzyadevych, C. Durrieu, J.-M. Chovelon, A bi-enzymatic whole cell conductometric biosensor for heavy metal ions and pesticides detection in water samples, Biosensors and Bioelectronics, 21(2005) 273-81.

[20] L. Cui, J. Wu, H. Ju, Electrochemical sensing of heavy metal ions with inorganic, organic and bio-materials, Biosensors and Bioelectronics, 63(2015) 276-86.

[21] L. Pujol, D. Evrard, K. Groenen-Serrano, M. Freyssinier, A. Ruffien-Cizsak, P. Gros, Electrochemical sensors and devices for heavy metals assay in water: the French groups' contribution, Frontiers in chemistry, 2(2014) 19.

[22] B. Bansod, T. Kumar, R. Thakur, S. Rana, I. Singh, A review on various electrochemical techniques for heavy metal ions detection with different sensing platforms, Biosensors and Bioelectronics, 94(2017) 443-55.

[23] A. Mason, B. Abdullah, M. Muradov, O. Korostynska, A. Al-Shamma'a, S.G. Bjarnadottir, et al., Theoretical basis and application for measuring pork loin drip loss using microwave spectroscopy, Sensors (14248220), 16(2016) 1-13.

[24] M.H. Zarifi, S. Deif, M. Abdolrazzaghi, B. Chen, D. Ramsawak, M. Amyotte, et al., A Microwave Ring Resonator Sensor for Early Detection of Breaches in Pipeline Coatings, IEEE Transactions on Industrial Electronics, 65(2018) 1626-35.

[25] J.W. Choi, J. Cho, Y. Lee, J. Yim, B. Kang, K. Keun Oh, et al., Microwave Detection of Metastasized Breast Cancer Cells in the Lymph Node; Potential Application for Sentinel Lymphadenectomy, Breast Cancer Research and Treatment, 86(2004) 107-15.

[26] M. Castro-Giráldez, M.C. Aristoy, F. Toldrá, P. Fito, Microwave dielectric spectroscopy for the determination of pork meat quality, Food Research International, 43(2010) 2369-77.

[27] A. Mason, O. Korostynska, S. Wylie, A.I. Al-Shamma'a, Non-destructive evaluation of an activated carbon using microwaves to determine residual life, Carbon, 67(2014) 1-9.

[28] M.H. Zarifi, M. Daneshmand, Liquid sensing in aquatic environment using high quality planar microwave resonator, Sensors and Actuators B: Chemical, 225(2016) 517-21.

[29] O. Korostynska, M. Ortoneda-Pedrola, A. Mason, A.I. Al-Shamma'a, Flexible electromagnetic wave sensor operating at GHz frequencies for instantaneous concentration measurements of NaCl, KCl, $MnCl_2$ and CuCl solutions, Measurement Science and Technology, 25(2014) 065105.

[30] S. Cashman, O. Korostynska, A. Shaw, P. Lisboa, L. Conroy, Detecting the presence and concentration of nitrate in water using microwave spectroscopy, IEEE Sensors Journal, PP(2017) 4092-4099.

[31] V. Ferrari, M. Prudenziati, 8 - Printed thick-film capacitive sensors, Printed Films, Woodhead Publishing2012, pp. 193-220.

[32] M. Prudenziati, Handbook of Sensors and Actuators,, 1st ed., Amsterdam, Elsevier Science, 1994.

[33] K. Arshak, I. Gaidan, Development of a novel gas sensor based on oxide thick films, Materials Science and Engineering: B, 118(2005) 44-9.

[34] R. Igreja, C.J. Dias, Dielectric response of interdigital chemocapacitors: The role of the sensitive layer thickness, Sensors and Actuators B: Chemical, 115(2006) 69-78.

[35] E. Reimhult, F. Höök, Design of Surface Modifications for Nanoscale Sensor Applications, Sensors (Basel, Switzerland), 15(2015) 1635-75.

[36] A. Azmi, A.A. Azman, K.K. Kaman, S. Ibrahim, S.C. Mukhopadhyay, S.W. Nawawi, et al., Performance of Coating Materials on Planar Electromagnetic Sensing Array to Detect Water Contamination, IEEE Sensors Journal, 17(2017) 5244-51.

[37] S. Sen Gupta, K.G. Bhattacharyya, Kinetics of adsorption of metal ions on inorganic materials: A review, Advances in Colloid and Interface Science, 162(2011) 39-58.

[38] I. Švancara, C. Prior, S.B. Hočevar, J. Wang, A Decade with Bismuth-Based Electrodes in Electroanalysis, Electroanalysis, 22(2010) 1405-20.

[39] N. Serrano, A. Alberich, J.M. Díaz-Cruz, C. Ariño, M. Esteban, Coating methods, modifiers and applications of bismuth screen-printed electrodes, TrAC Trends in Analytical Chemistry, 46(2013) 15-29.

[40] G.H. Hwang, W.K. Han, J.S. Park, S.G. Kang, An electrochemical sensor based on the reduction of screen-printed bismuth oxide for the determination of trace lead and cadmium, Sensors and Actuators, B: Chemical, 135(2008) 309-16.

[41] R.O. Kadara, N. Jenkinson, C.E. Banks, Disposable Bismuth Oxide Screen Printed Electrodes for the High Throughput Screening of Heavy Metals, Electroanalysis, 21(2009) 2410-4.

[42] I. Frau, O. Korostynska, P. Byrne, A. Mason, Feasibility of in-situ quality assessment of zinc contamination in water, 2017, IEEE First Ukraine Conference on Electrical and Computer Engineering (UKRCON), Kiev, pp. 249-522017, pp. 249-52.

[43] A.O. Dada, A. Olalekan, A. Olatunya, D.O. Dada, Langmuir, Freundlich, Temkin and Dubinin-Radushkevich isotherms studies of equilibrium sorption of Zn2+ unto phosphoric acid modified rice husk, IOSR Journal of Applied Chemistry 3(2012) 38-45.

[44] I. Frau, S. Wylie, J. Cullen, O. Korostynska, P. Byrne, A. Mason, Microwaves and Functional Materials: A Novel Method to Continuously Detect Metal Ions in Water, in: S.C. Mukhopadhyay, K.P. Jayasundera, O.A. Postolache (Eds.), Modern Sensing Technologies, Springer International Publishing, Cham, 2019, pp. 179-201.

[45] Z. Chu, J. Peng, W. Jin, Advanced nanomaterial inks for screen-printed chemical sensors, Sensors and Actuators B: Chemical, 243(2017) 919-26.

[46] S. Patil, V. Puri, Effect of bismuth oxide thick film overlay on microstrip patch antenna, Microelectronics International, 27(2010) 79-83.

[47] T. Chen, S. Li, H. Sun, Metamaterials Application in Sensing, Sensors, 12(2012) 2742.

[48] C. Bernou, D. Rebière, J. Pistré, Microwave sensors: a new sensing principle. Application to humidity detection, Sensors and Actuators B: Chemical, 68(2000) 88-93.

[49] S.F.L. Lynch, L.C. Batty, P. Byrne, Critical control of flooding and draining sequences on the environmental risk of Zn-contaminated riverbank sediments, J Soils Sediments, (2017).

[50] R. Cidu, F. Frau, S. Da Pelo, Drainage at Abandoned Mine Sites: Natural Attenuation of Contaminants in Different Seasons, Mine Water and the Environment, 30(2011) 113-26.

[51] M. Kohl, G. Veltl, M. Busse, Printed Sensors Produced via Thick-film Technology for the Use in Monitoring Applications, Procedia Technology, 15(2014) 107-13.

# Supplementary material

## *Detection of Zn in water using novel functionalised planar microwave sensors*

Ilaria Frau[a]*, Steve Wylie[a], Patrick Byrne[b], Jeff Cullen[a], Olga Korostynska[c], Alex Mason[a,d,e]

[a]Faculty of Engineering and Technology, Liverpool John Moores University, Liverpool L3 3AF, UK

[b]Faculty of Science, Liverpool John Moores University, Liverpool L3 3AF, UK

[c]Faculty of Technology, Art and Design, Department of Mechanical, Electronic and Chemical Engineering, Oslo Metropolitan University, Oslo, Norway

[d]Animalia AS, Norwegian Meat and Poultry Research Centre, PO Box Økern, 0513 Oslo, Norway

[e]Faculty of Science and Technology, Norwegian University of Life Sciences, 1432 Ås, Norway

[*]i.frau@2016.ljmu.ac.uk, Byrom Street, Liverpool L3 3AF, UK

**Table S1** Specific conductivity of the Zn solutions.

| Zn solutions (mg/L) | Specific conductivity (mS/cm) |
|---|---|
| **0** | 0.0021 |
| **0.1** | 0.0141 |
| **0.5** | 0.0711 |
| **1** | 0.1313 |
| **10** | 1.326 |
| **50** | 6.53 |
| **100** | 13.06 |

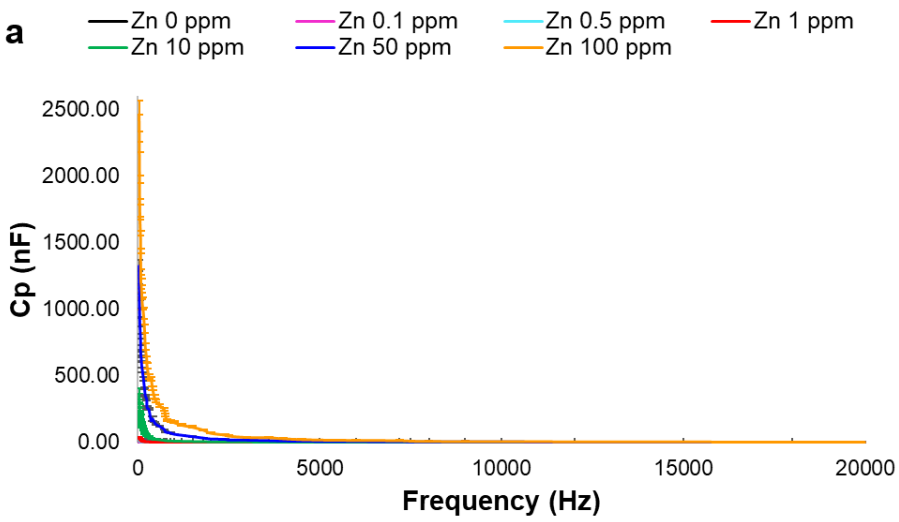


1

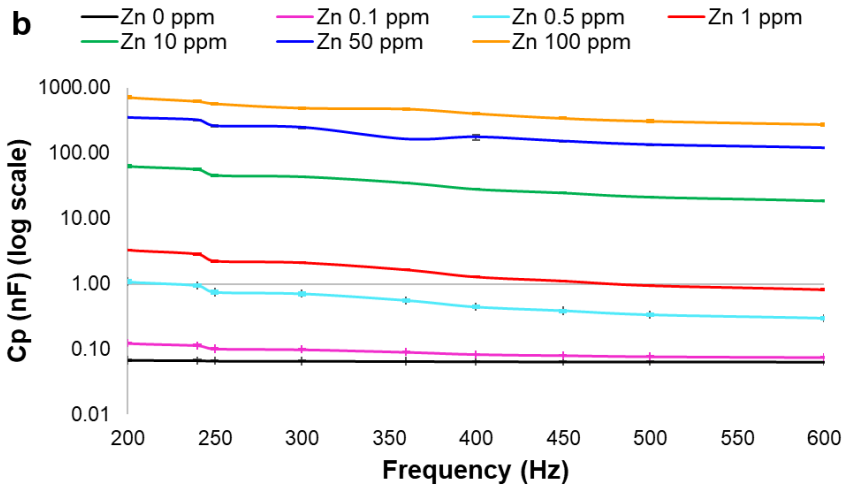


2

3 **Fig. S6.** Spectral response for (**a**) capacitance ($C_p$) and Zn solutions at low frequency (20 Hz – 20 kHz) and (**b**) its enlargement in the
4 frequency range 200-600 Hz for a clearer view of the selected frequency with $C_p$ espressed with log scale for showing also the Zn
5 concentration < 1 mg/L.

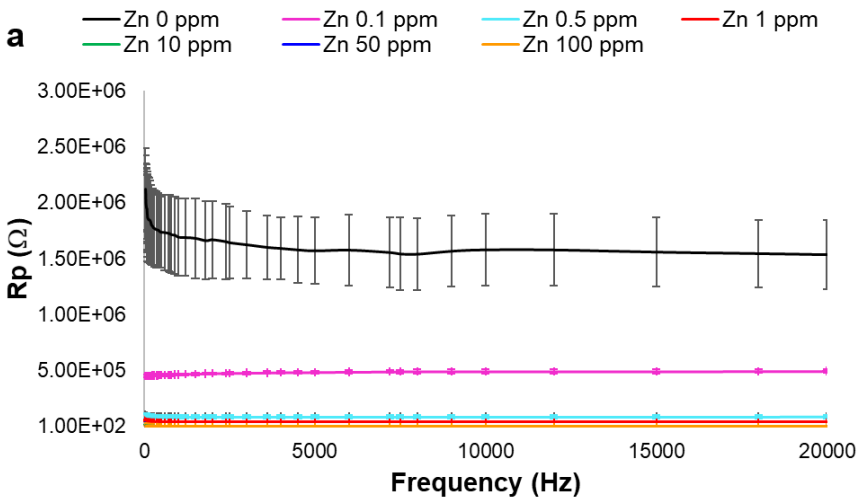


6

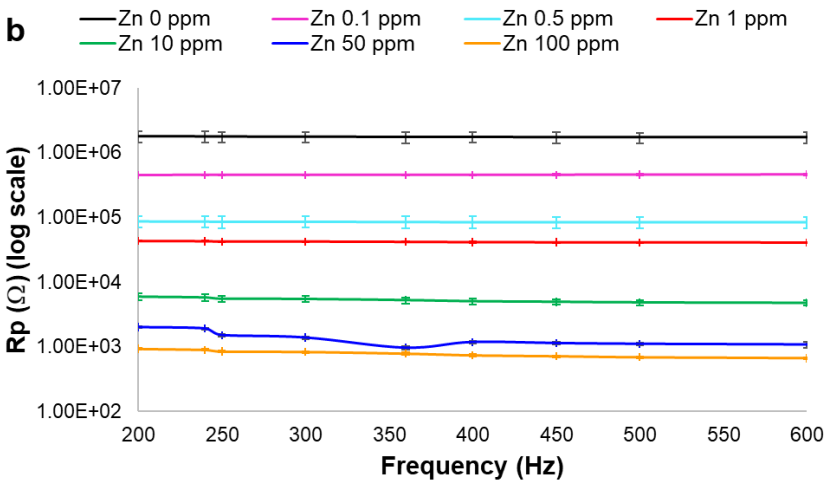


**Fig. S2.** Spectral response for (**a**) resistance ($R_p$) and Zn solutions at low frequency (20 Hz – 20 kHz) and (**b**) its enlargement in the frequency range 200-600 Hz for a clearer view of the selected frequency with $R_p$ espressed with log scale for showing also the Zn concentration < 1 mg/L.

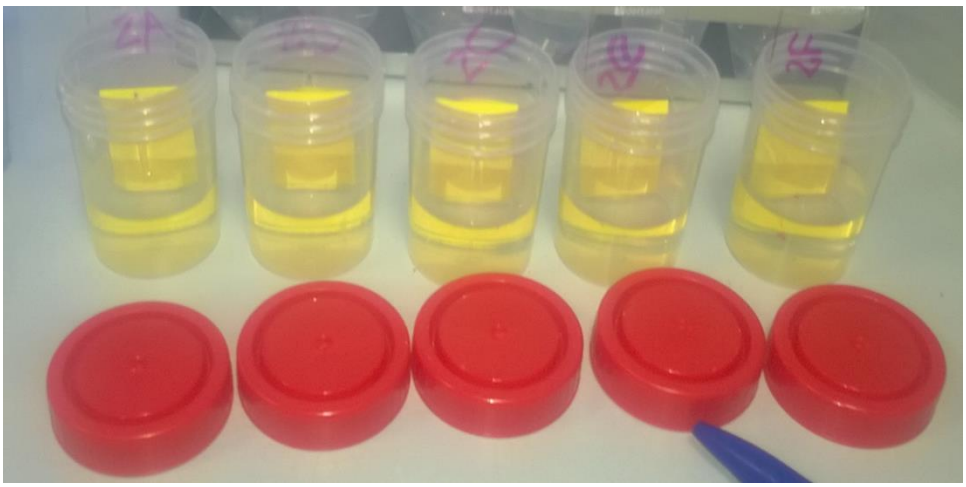

**Fig. S3.** Experimental procedure for measuring the adsorption of Zn ions on the coatings based on $Bi_2O_3$: thick-films printed on microscope slides were immersed on the Zn solutions and the concentration was measured after 5 and 10 minutes.

**Table S2** The absorption of Zn onto coatings was estimated by adding the coating material printed on a microscope slide on each Zn solution and measuring the concentration of it after 5 and 10 min using a conductivity meter ($R^2$= 1 for Zn concentration 0-100 mg/L).

| | **Conductivity (mS/cm ) after** | | **Concentration (mg/L ) after** | | **Adsorption (%) after** | |
|---|---|---|---|---|---|---|
| **Zn solutions (mg/L)** | **5 min** | **10 min** | **5 min** | **10 min** | **5 min** | **10 min** |
| **0** | 0.0021 | 0.0023 | 0 | 0 | 0 | 0 |
| **0.1** | 0.0135 | 0.0132 | 0.0957 | 0.9362 | 4.3 | 6.4 |
| **0.5** | 0.0681 | 0.0667 | 0.4479 | 0.4789 | 4.2 | 6.2 |
| **1** | 0.1261 | 0.1235 | 0.0957 | 0.9337 | 4.0 | 5.9 |
| **10** | 1.234 | 1.211 | 9.611 | 9.435 | 3.9 | 5.7 |
| **50** | 6.279 | 6.162 | 48.07 | 47.18 | 3.8 | 5.6 |
| **100** | 12.58 | 12.39 | 96.32 | 94.87 | 3.7 | 5.1 |

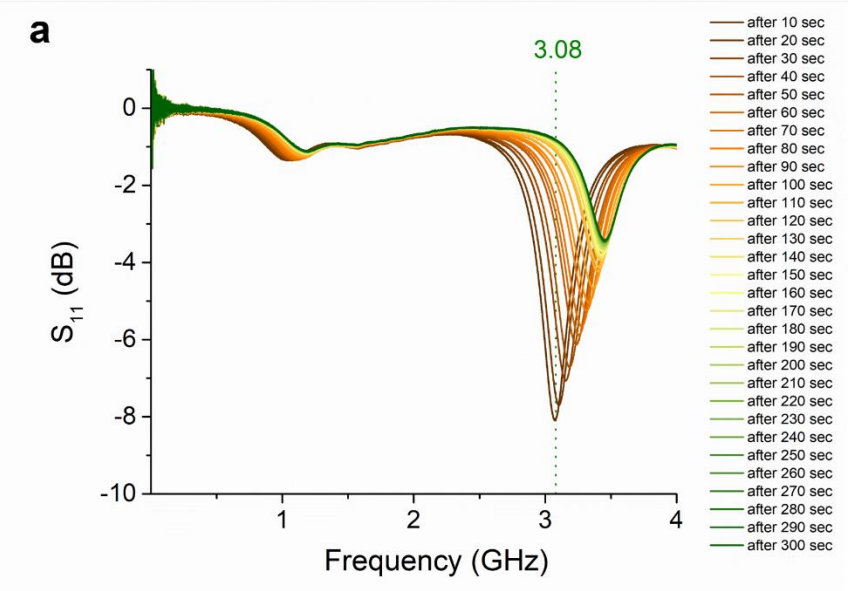


1

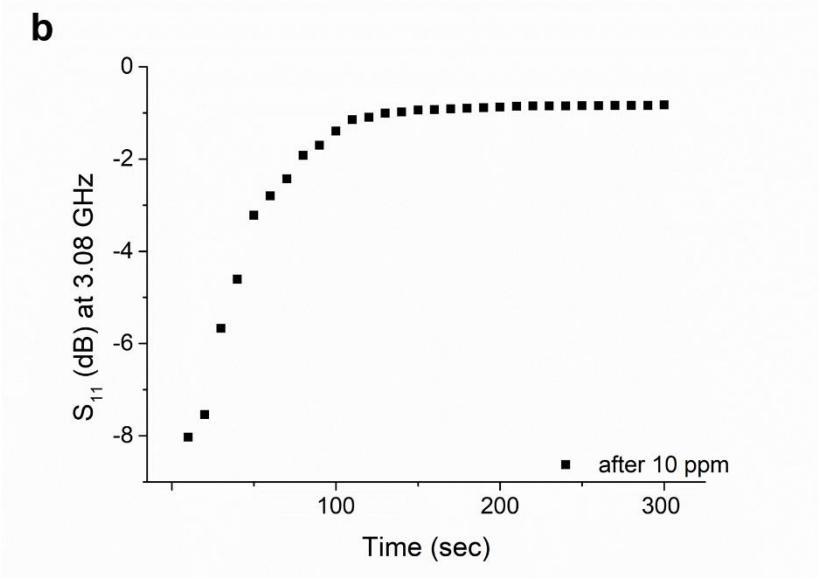


2

3 **Fig. S4.** (**a**) F-EM sensor spectra by time (every 10 seconds) measured after the interaction of 10 mg/L of Zn; (**b**) the correlation at 3.08
4 GHz between recovery time and $S_{11}$ response show stability and the return to the "air" spectrum is reached between 100-150 seconds.

5